Topological Superconductivity in Doped Magnetic Moiré Semiconductors

Valentin Crépel, Daniele Guerci, Jennifer Cano, J. H. Pixley, and Andrew Millis

Phys. Rev. Lett. **131**, 056001 — Published 1 August 2023

DOI: 10.1103/PhysRevLett.131.056001

Topological superconductivity in doped magnetic moiré semiconductors

Valentin Crépel,[1,*] Daniele Guerci,[1,*] Jennifer Cano,[2,1] J. H. Pixley,[3,1] and Andrew Millis[4,1]

[1] *Center for Computational Quantum Physics, Flatiron Institute, New York, New York 10010, USA*
[2] *Department of Physics and Astronomy, Stony Brook University, Stony Brook, New York 11794, USA*
[3] *Department of Physics and Astronomy, Center for Materials Theory, Rutgers University, Piscataway, New Jersey 08854, USA*
[4] *Department of Physics, Columbia University, New York, NY 10027, USA*

We show that topological superconductivity may emerge upon doping of transition metal dichalcogenide heterobilayers above an integer-filling magnetic state of the topmost valence moiré band. The effective attraction between charge carriers is generated by an electric p-wave Feshbach resonance arising from interlayer excitonic physics and has a tuanble strength, which may be large. Together with the low moiré carrier densities reachable by gating, this robust attraction enables access to the long-sought p-wave BEC-BCS transition. The topological protection arises from an emergent time reversal symmetry occurring when the magnetic order and long wavelength magnetic fluctuations do not couple different valleys. The resulting topological superconductor features helical Majorana edge modes, leading to half-integer quantized spin-thermal Hall conductivity and to charge currents induced by circularly polarized light or other time-reversal symmetry-breaking fields.

Introduction — Topological p-wave superconductors are predicted to exhibit interesting properties that inherently differ from those of topologically trivial superconductors [1–4]. Most notoriously, they host Majorana modes [5–7] that are key to realizing a topological quantum computer [2]. They also feature boundary thermal currents topologically protected from disorder-induced backscattering, producing essentially dissipationless thermal channels on the surface and excellent thermal conductors. Despite intensive efforts [8, 9], topological superconductivity (TS) remains elusive, and material candidates are largely limited to fine-tuned non-stochiometric compounds [10–15] that inevitably suffer from defects that make there identification elusive. The recent advent of gate-tunable moiré heterostructures allows one to bypass this unfavorable condition, and at the same time offers a unique context for intertwined topology and superconductivity [16–25].

Here, we propose a clear route towards achieving time-reversal-invariant topological p-wave superconductivity in transition metal dichalcogenide (TMD) moiré heterobilayers. The TS arises in the weakly doped layer-transfer regime; where one layer contains one hole per moiré unit cell, forming a Mott insulator with a large gap to in-layer charge excitations, and an additional $x \ll 1$ carriers are added to the other layer, forming a dilute Fermi liquid. This regime has recently been reached in $MoTe_2/WSe_2$ heterobilayers [26], where coexistence of local moments and itinerant carriers was reported [27–29].

For the physics addressed in this letter, the crucial feature of TMD moiré bilayers is their strong interlayer Coulomb interaction, which leads to a remarkable range of (charged) interlayer excitons that strongly couple to mobile carriers. For example, full experimental control over electron-exciton scattering in TMD bilayers

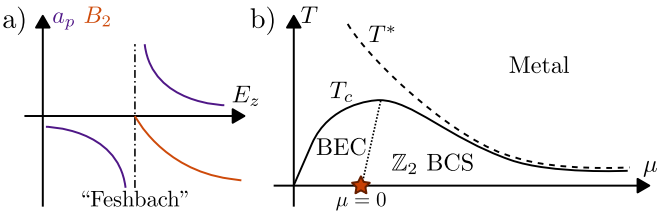

FIG. 1. a) An out-of-plane electric field E_z can change the sign of a_p, the p-wave scattering length between doped charge. This solid-state Feshbach resonance yields bound states of energy $B_2 < 0$ below the band bottom when $a_p > 0$ [40, 41]. b) Schematic phase diagram predicted for AA-stacked TMD heterobilayers as a function of chemical potential μ, which can be varied by electrostatic gating. Below the BKT temperature T_c, the system either evolves into a $\mathbb{Z}_2$ topological superconductor ($\mu \gtrsim 0$) or a gapped Bose-Einstein condensate of pairs ($\mu \lesssim 0$). They are separated by a crossover at finite-temperature (dots), which becomes a phase transition at $T = 0$ (star) [42–44]. For large μ, T_c almost matches the pair binding T^* (dashes).

was recently demonstrated through interlayer trion dressing [30], whose electric field dependent energy enabled scanning across a Feshbach resonance of this composite system [31, 32]. In our theory, the crucial role is played by a low-lying charge-$2e$ interlayer exciton (quaternion), also recently probed by spectroscopy in TMD bilayers [33]. This low-lying virtual state's contribution to electron scattering may be described in terms of an effective p-wave scattering length a_p between doped charges that changes sign under electrostatic gating (see Fig. 1a). Proximity to this Feshbach resonance provides the strong interaction necessary for the emergence of robust superconductivity. Independent of superconductivity, it is important to note that this p-wave electric Feshbach resonance is a solid-state realization of a phenomenon that is still intensely looked for in ultracold gases [34–39].

The physics of the weakly-doped layer-transfer regime

[*] These authors contributed equally.

is rich, with many different phases and phenomena depending on the stacking, interlayer potential and hybridization configurations. In this paper we focus on the arrangement of most interest for topological superconductivity, namely, AA-stacked bilayers with interlayer hybridization comparable to but weaker than the interlayer potential difference, which is in turn weaker than the interaction scales. The AB-stacked case and more general parameter regimes will be presented elsewhere [45]. In the case targeted here, the layer hybridization couples the itinerant carriers in the lightly doped layer to excitons, providing the p-wave pairing, and also leads to ferromagnetic order in the Mott insulating layer. This ferromagnetic order does not couple the Fermi pockets of the lightly doped layer, implying an emergent $\mathbb{Z}_2$ time-reversal symmetry that promotes the p-wave superconducting state to the topologically protected DIII class [46]. The clear physical consequence is a pair of gapless counter-propagating (helical) Majorana edge modes.

Because the pairing depends on parameters independent of the Fermi surface and remains strong even in the very low density limit, we expect that the low carrier densities reachable by gating in moiré heterostructures enables access to the full evolution from weakly bound Cooper pairs forming a $\mathbb{Z}_2$ topological superconductor ($\mathbb{Z}_2$ BCS regime) to a Bose-Einstein condensate of tightly bound pairs (BEC regime), as sketched in Fig. 1b.

Model — Lattice parameter mismatch means that stacking two inequivalent TMD layers at zero or nonzero twist angle will create a moiré pattern with a unit cell that is large relative to atomic dimensions. Extensive experimental [22, 47] and theoretical [48–53] studies have established that the low energy physics of this situation may be described by a generalized Hubbard model $H = H_{\rm int} + H_{uu} + H_{dd} + H_{ud}$ involving two interpenetrating triangular lattices (one for each layer) featuring in-layer H_{uu}, H_{dd} and interlayer H_{ud} nearest neighbor hoppings [52], in-layer interactions U_u, U_d and an interlayer interaction V (see Fig. 2a). The hopping terms are

$$H_{ab} = -t_{ab} \sum_{\langle i,j\rangle_{ab}} c_i^\dagger e^{-i\sigma^z \nu_{ij}^{ab} \varphi_{ab}} c_j, \qquad (1)$$

with $(a,b) \in \{u,d\}$ denoting the up or down layer, (i,j) labelling orbitals in these layers, and $\langle i,j\rangle_{ab}$ denoting nearest neighbor pairs having $i \in a$ and $j \in b$ (see Fig. 2a). We have written the fermionic operator for holes as two-component spinors $c_j^\dagger = [c_{j,K}^\dagger, c_{j,K'}^\dagger]$, labelled by the spin-valley locked degrees of freedom of the two wannierized TMDs. The hopping parameters are in general complex [23]; in the AA-stacked configuration studied here, we may choose the interlayer hopping parameters to be real ($\varphi_{ud} = 0$) and set $\varphi_{uu} = \varphi_{dd} = 2\pi/3$ with $\nu_{ij} = +1$ when the link $i \to j$ turns right and $\nu_{ij} = -1$ otherwise. In this convention, the t_{ab} are real and positive. The intra-layer hopping phases of $2\sigma^z\pi/3$ are imposed by the rotation symmetry of the continuum

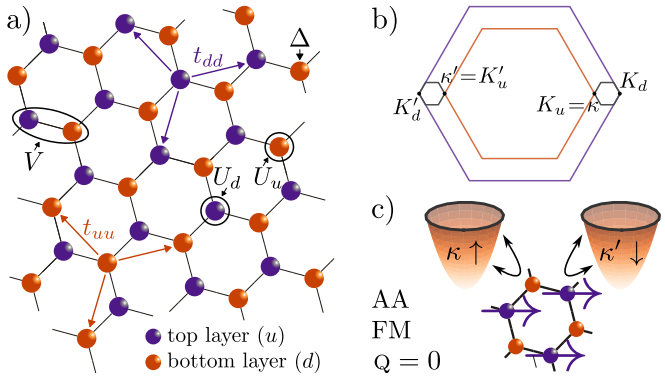

FIG. 2. a) Wannierized model of TMD heterobilayers (Eqs. 1&2) keeping the dominant intra- and inter-layer interactions (U_d, U_u and V) and tunnelings. The phases $\varphi_{uu} = \varphi_{dd} = 2\pi/3$ of the tunnelings are depicted by arrows for the K spin-valley component. b) Folding of the monolayer $\pm K_{u/d}$ points onto the mini-Brillouin zone corners κ and κ'. c) If the magnetic state stabilized at filling $n_h = 1$ is am in-plane ferromagnet, it cannot induce low-energy spin-flips due to spin-valley locking of the charge carriers described by parabolic dispersion around κ and κ'.

model from which they derive [52], and can also be understood as the dynamical phases that spin-valley locked holes with momentum $\sigma^z K$ acquire upon translation by a moiré lattice vector [54]. The interaction terms may be written

$$H_{\rm int} = \Delta \sum_{i\in u} n_i + \sum_{a,i\in a} U_a n_{i,\uparrow} n_{i,\downarrow} + V \sum_{\langle i,j\rangle_{ud}} n_i n_j. \qquad (2)$$

The interlayer potential difference Δ is about 0.1 eV for the $MoTe_2/WSe_2$ system of immediate experimental relevance, and may be tuned by an out-of-plane electric field [55, 56].

Representative values estimated from a continuum model for $MoTe_2/WSe_2$ bilayers [51] are $U_d \approx 90\,\text{meV} \gtrsim \Delta$, $U_u \approx 74\,\text{meV}$ and $V \approx 44\,\text{meV}$, the large size of the moiré unit cell relative to the interplane separation explaining $V \sim U_{u,d}$. The superconducting state discussed in this work appears when V exceeds $\Delta/4$ (see below). The interaction strength increases with increasing V until V becomes so large that the charge transfer gap exceeds the Mott gap and the doped holes go into the magnetic layer.

Magnetic coupling — We investigate the physics of the Hamiltonian defined by Eqs. 1 and 2 in the layer-transfer limit $t \equiv t_{ud} \ll \Delta \ll \Delta + 3V < U_d$. In this regime, carriers added up to a density of one hole per moiré unit cell go into the lower layer and due to the large U_d form a Mott insulator at the density $n_h = 1$, while a small density x of carriers added beyond $n_h = 1$ will go into the upper plane. We now consider the interactions affecting these x extra carriers.

When $U_d \gg \Delta$, the leading magnetic interaction is a trion-mediated exchange which, combined with the strong single-layer spin orbit coupling, leads to xy-

ferromagnetism in the Mott layer [25]. In-plane magnetism in the lower level acts as a spin-flip operator for carriers in the upper layer. However, the spin-valley locking in the monolayers, transferred to the moiré $\pm\kappa$ valleys after folding their large Brillouin zone onto the small moiré one (see Fig. 2b), means that low energy spin-flips involve momentum transfers of the order of $\kappa - \kappa'$. For this reason, a small density of carriers doped above the Mott insulating state cannot undergo spin-flip scattering from the ferromagnetic order or its low-lying spin wave excitations at low-energy (see Fig. 2c). As a result, the bottom layer effectively behaves as a featureless charge reservoir. As a result, the low-energy carriers located in the upper layer enjoy an emergent time reversal symmetry (TRS) $T = i\tilde{\sigma}^y K$ and the full U(1) spin-rotation symmetry generated by $\tilde{\sigma}^z$, although both are spontaneously broken by the Mott state. Here, $\tilde{\sigma}$ denotes the spin-valley Pauli matrices projected to the active modes $[\psi^\dagger_{q,\Uparrow}, \psi^\dagger_{q,\Downarrow}]$ near the top of the valence band, with $\Uparrow$ / $\Downarrow$= $(\kappa/\kappa', \uparrow / \downarrow)$. The system features two spin-valley locked hole pockets with dispersion $\varepsilon_q = q^2/2m$ [57], shown in Fig. 2c, related by the emergent TRS.

Equal-spin pairing instability — Since carriers near the Fermi surface (FS) only couple to the density of the insulating bottom layer, our system is an experimentally viable realization of the setup recently discussed in terms of model systems to describe a repulsive mechanism for superconductivity [58–62]. This mechanism relies on the existence of a charge-2e exciton (quaternion) with lower energy than all charge e and neutral excitations of the system at $t = 0$, which is achieved thanks to the large V of our model. This quaternion provides a closed scattering channel that can be virtually occupied by pairs of mobile carriers to obtain a non-zero binding energy (see Fig. 3a), in direct analogy to the physics of Feshbach resonance.

The effective attraction is explicitly seen when the interaction term of our lattice model is projected onto the active modes at low doping, retaining pair operators with relative form factor of zeroth or first order in the small momentum deviations away from $\pm\kappa$ [57]

$$\mathcal{H}^{\rm int}_{k,k'} = g_s \mathcal{S}^\dagger_k \mathcal{S}_{k'} + \sum_{\ell s} (g_t - \ell s g'_t) \left(\mathcal{T}^{\ell s}_k\right)^\dagger \mathcal{T}^{\ell s}_{k'}, \quad (3)$$

where $\mathcal{S}_k = (\psi_{-k,\Uparrow}\psi_{k,\Downarrow} - \psi_{-k,\Downarrow}\psi_{k,\Uparrow})/\sqrt{2}$ denotes the s-wave pair operator, while $\mathcal{T}^{\ell-}_k = k_\ell \psi_{-k,\Downarrow}\psi_{k,\Downarrow}$, $\mathcal{T}^{\ell 0}_k = k_\ell(\psi_{-k,\Uparrow}\psi_{k,\Downarrow} + \psi_{-k,\Downarrow}\psi_{k,\Uparrow})/\sqrt{2}$ and $\mathcal{T}^{\ell+}_k = k_\ell \psi_{-k,\Uparrow}\psi_{k,\Uparrow}$ describe p-wave pairs of spin $s = -1, 0, +1$, respectively. Their orbital angular momentum $\ell = \pm$ is fixed by their form factors $k_\pm = k_x \pm i k_y$. As claimed, the g-coefficients extracted from second order perturbation theory [57], plotted in Fig. 3b, unveil attractive interactions in the p-wave channel of our model for large enough V/Δ [57]. The s-wave scattering amplitude receives a contribution from the large on-site repulsion and therefore remains positive, $g_s \sim U_u > 0$, impeding an s-wave superconducting order. The largest negative interaction strength is found in the $\{\mathcal{T}^{-+}, \mathcal{T}^{+-}\}$ sector, which describes valley-chirality locked $p \pm ip$ equal-spin pairing. The remaining triplet channels feature similar form factors and subleading attraction strengths (Fig. 3b), and can thus be safely ignored.

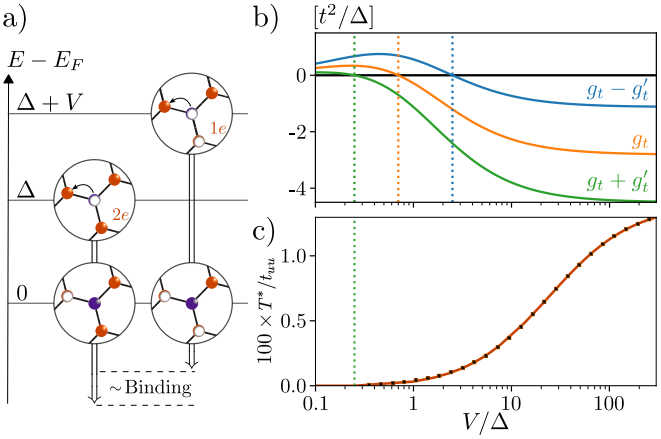

FIG. 3. a) The lowest excitation with which isolated carriers (orange) hybridize has higher energy than the charge $2e$ excitons that couples to pairs of carriers. This offers a strong energy reduction to pairs and can produce a non-zero binding energy. b) Interaction coefficients in the different p-wave channels (Eq. 3) with dotted lines marking the value of V/Δ above which they become negative – 1/4 for the leading pairing channel. c) The pair binding energy T^* is non-zero above this value, and increases with V/Δ from small to large values compared to the Fermi energy E_F, describing a BCS to BEC evolution. The solid and dotted lines respectively show numerical estimates and results from a generic p-wave BCS formula, both obtained for $x = 0.1$, $t_{uu} = \Delta$ and $t^2/(\Delta t_{uu}) = 0.25$.

The pair binding energy T^* extracted from the log-singularity of the particle-particle susceptibility in these channels is shown in Fig. 3c [57]. It perfectly agrees with the generic BCS-like formula for p-wave attraction $k_B T_c \propto \exp[-1/(\rho E_F \tilde{g})]$ [63], where $\tilde{g} = 4\rho|g_t + g'_t|/\pi$ is the dimensionless attraction strength in the dominant pairing channel, and $\rho = m/(2\pi\hbar^2)$ the constant density of states near the band bottom [64]. Continuum model calculations give the gap-to-T^* ratio $2\Delta_{\rm sc}/(k_B T^*) \approx 3$.

$\mathbb{Z}_2$ topological superconductor — We now show that the emergent low-energy TRS of doped holes grants topological protection to the superconducting state, resulting in pairs of helical Majorana modes on its edges. Introducing the bosonic fields $\phi_\pm$ to describe the superconducting order parameters in the $\mathcal{T}^{\pm\mp}$ channels, and performing a Hubbard-Stratonovitch transformation, we obtain the Bodgoliubov-de Gennes (BdG) Hamiltonian

$$\mathcal{H}^{\rm BdG}_q = \frac{1}{2}\begin{bmatrix} h_q & \Delta_q \\ \Delta_q^\dagger & -h_q \end{bmatrix}, \quad \Delta_q = \begin{bmatrix} 0 & \phi_+ q_+ \\ \phi_- q_- & 0 \end{bmatrix}, \quad (4)$$

expressed in Nambu space $[\psi_{q,\Uparrow}, \psi_{q,\Downarrow}, \psi^\dagger_{-q,\Downarrow}, \psi^\dagger_{-q,\Uparrow}]$, with $h_q = q^2/2m - \mu$ and μ the chemical potential. The block structure of $\mathcal{H}^{\rm BdG}$ translates into a decoupled sum of free

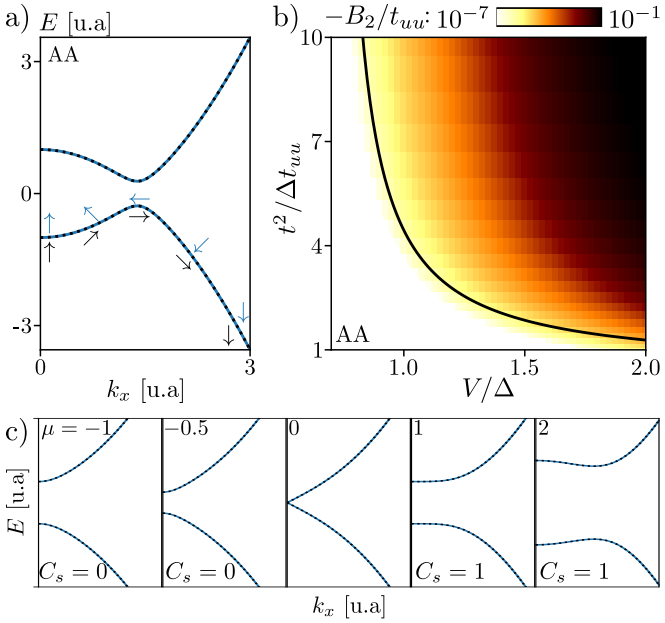

FIG. 4. a) BdG band structure for the superconducting state. The non-trivial and opposite winding of the Nambu vectors of the lower bands n_q^s, shown with arrows, signals a non-zero spin Chern number. b) Pairing persists down to the two-particle level for certain choices of parameters, as indicated by a negative binding energy $B_2 < 0$. The black lines show the separation between the regions with and without bound states below the carrier band edge obtained from the effective continuum theory Eq. 3. c) The evolution from BEC (left) to BCS (right) at zero temperature involves a topological phase transition, illustrated here using the BdG band structure as a function of the chemical potential μ. C_s denotes the spin Chern number of the negative-energy BdG bands.

energies for the $\Uparrow$ / $\Downarrow$ sectors $\mathcal{F} = \sum_{a=\pm}(\alpha|\phi_a|^2 + |\phi_a|^4)$. Below T_c, *i.e.* for $\alpha < 0$, the minimization of $\mathcal{F}$ implies that both species be equally populated $|\phi_+| = |\phi_-|$ [57]. Up to an irrelevant gauge choice, we thus have $\phi_+ = \phi_-^* = \phi e^{i\theta}$.

The two spin-valley components of $\mathcal{H}^{\mathrm{BdG}}$ decouple into time-reversal conjugated 2×2 blocks that can be written using Nambu Pauli matrices $\vec{\tau}$ as $\mathcal{H}_q^s = E_q \vec{n}_q^s \cdot \vec{\tau}$ with $E_q^2 = h_q^2 + |\phi q|^2$. As illustrated in Fig. 4a, the unit vectors $n_q^s = [\phi\,(R_\theta q)_x\,, s\phi\,(R_\theta q)_y\,, h_q]/E_q$, where R_θ is the rotation matrix by angle θ around the z-axis, fully wrap around the Bloch sphere as momentum is varied provided $\mu > 0$. This ensures a non-zero Chern number to all four Bogoliubov bands. Since the vectors n_q^s are mirrors of one another with respect to the (xz) plane for opposite spin $s = \pm$, the Chern numbers for the two hole-like Bogoliubov bands are opposite. They hence carry a non-trivial spin Chern number $C_s = 1$.

The existence of this spin-Chern number follows from the particle-hole operator $\mathcal{P} = \tilde{\sigma}^0\tau^x$ acting as $\mathcal{P}\mathcal{H}_q^{\mathrm{BdG}}\mathcal{P} = -\mathcal{H}_{-q}^{\mathrm{BdG}}$ and an additional chiral symmetry $\mathcal{O} = \tilde{\sigma}^z\tau^z$ that commute with $\mathcal{H}_q^{\mathrm{BdG}}$ which imply that the state belongs to the DIII class of the Altland-Zirnbauer classification [46] and the obtained triplet superconducting state is topologically protected. The topological phase displays a superposition of $p \pm ip$ superconducting components [65], easily anticipated given the form of Δ_q in Eq. 4. More remarkable is the existence of counter-propagating chiral Majorana modes at the edge of the system, described by

$$\mathcal{L} = i\chi_{\Uparrow}(\partial_t - \partial_x)\chi_{\Uparrow} + i\chi_{\Downarrow}(\partial_t + \partial_x)\chi_{\Downarrow}, \qquad (5)$$

where $\chi_{\Uparrow} = u\psi_{\Uparrow} + u^*\psi_{\Uparrow}^\dagger$ and $\chi_{\Downarrow} = u^*\psi_{\Downarrow} + u\psi_{\Downarrow}^\dagger$, with u the normalized hole component of the $\Uparrow$ band of $\mathcal{H}_q^{\mathrm{BdG}}$ [2]. This pair of helical edge modes is protected by $\mathcal{O}$, for which they are eigenmodes with opposite eigenvalues.

The obtained $\mathbb{Z}_2$ topological superconductor can be revealed by a half-integer value of the spin-thermal Hall conductivity, coming from the Majorana edge modes [3]. While spin-thermal Hall currents have not yet been measured, any TRS breaking perturbation, *e.g.* circularly polarized light, can imbalance the population in the two valleys and confer properties akin to chiral p-wave superconductors, which can be probed through electric currents [66]. In addition, Majorana zero modes in vortex cores [3] could be observed with scanning tunneling microscopy as zero-bias peaks [67].

Beyond its topological protection, another interesting feature arises from the large momentum transfer $\kappa - \kappa'$ required to coherently scatter holes between the two valleys, which prevents any quartic term besides the residual pair repulsion from appearing in the Ginzburg free energy [57]. The lowest order term coupling the phases of ϕ_+ and ϕ_- is thus of sixth order $(\phi_+^*)^3\phi_-^3 + hc$. This high order term induces a noteworthy third-order Josephson effect with distinctive low-energy Leggett modes [68].

p-wave BEC-BCS transition — T^* in Fig. 3c only matches the BKT transition temperature T_c in the weak-coupling regime $E_F \gg |g_t + \tilde{g}_t|$ [63]. In the opposite strong-coupling limit, *i.e.* at doping concentrations $x = 2\rho E_F < \rho|g_t + \tilde{g}_t|$, our model still exhibits pairing in some regime of parameters. To see this, we consider the binding energy of two charge carriers doped above the magnetic state $B_2 = E_2 - 2E_1 + E_0$, E_N denoting the ground state energy for N doped charges.

We first obtain B_2 as a function of the original parameters of the model by solving an effective lattice model containing all second order processes in t/Δ [57]. The results of this calculation are presented in Fig. 4b, and show the following trend: as Δ is decreased, *e.g.* by application of an out-of-plane electric field, the ratios V/Δ and $t^2/t_{uu}\Delta$ increase up to a critical point where bound states emerge $B_2 < 0$. This can be seen as a condensed-matter analog of a Feshbach resonance, where the non-retarded interaction between two fermions can be tuned from positive to negative using an externally controllable parameter. From a low-energy scattering perspective, this can be understood as tuning the p-wave scattering length a_p from negative to positive. The universal relation $B_2 \sim \hbar^2/ma_p^2\log(r/a_p)$ holds when $a_p > 0$ [40, 41],

where r is the range of p-wave interactions, comparable to the lattice constant.

The presence of bound pairs at infinitesimal doping offers access to the full evolution from a BEC of pairs to the BCS superconducting state, studied above in the weak coupling limit (Fig. 3). This evolution should be distinguished from the s-wave case in several ways. For p-wave interactions, the BCS and BEC regions are separated by a transition, *i.e.* by a gap closing [69], while it is a smooth crossover for s-wave interactions [70]. This is easily observed in our BdG Hamiltonian, whose eigenenergies vanish at $\mu = q = 0$ even when $\phi > 0$ remains finite. This gap closure, highlighted in Fig. 4c, separates the BCS regime $\mu > 0$ from the BEC regime $\mu < 0$. Another difference is that the physics in the p-wave case necessarily involves another length-scale in addition to the scattering length [69, 71].

In our specific model, the topological protection of the superconducting state in the FM case endows the BEC-BCS transition with a topological character. This is understood from the spin-split BdG Hamiltonians $\mathcal{H}^s_q$, which exhibit a textbook example of a band-inversion when the "mass" μ crosses zero energy [72]. The topological properties of the superconducting state are lost at any finite temperature due to thermal proliferation of topological excitations [42–44], and as a result the $T = 0$ transition into a crossover at any finite temperature.

Conclusion — We have exposed physical mechanisms leading to the emergence of a robust attraction and a low-energy time-reversal symmetry in transition metal dichalcogenides moiré heterobilayers featuring an in-plane ferromagnetic insulating state at integer filling, which together produce a time-reversal-invariant topologically protected p-wave superconductor at sufficiently low temperatures. The topological properties are inherited from the strong spin-orbit coupling of the original monolayers, when the latter is preserved by the magnetic Mott state. To provide experimental guidance we summarize the regime of parameters where pairing is predicted. The attraction relies on the large interlayer interaction V of the bilayer, takes place when $V > \Delta/4$, and increases with V/Δ, *e.g.* when electrostatic gating reduces the valence band offset Δ between layers and brings the quaternion excitation closer to the Fermi level. The value of the interactions $U_{u/d}$ and V are tunable by controlling the distance of the sample from the metallic gates and changing the energy offset Δ. For our theory to apply, the layer-transfer gap should also remain smaller than the in-layer Mott gap at filling one, leading to the electrostatic condition $U_u > \Delta + 3V$. All these scales can, in principle, be experimentally probed by scanning-tunneling microscopy or compressibility measurements to provide experimental guidance on how to reach the regime of interest for superconductivity.

Acknowledgments — D.G. thanks Michele Fabrizio for correspondence at the early stage of the work. V.C. is grateful to A. Imamoglu for an insightful discussion shaping some of the ideas presented here. We also acknowledge enlightening discussions with Chetan Nayak. This work was partially supported by the Air Force Office of Scientific Research under Grant No. FA9550-20-1-0260 (J.C.) and Grant No. FA9550-20-1-0136 (J.H.P.) and the Alfred P. Sloan Foundation through a Sloan Research Fellowship (J.C., J.H.P.). A.J. M. acknowledges support from the NSF MRSEC program through the Center for Precision-Assembled Quantum Materials (PAQM) NSF-DMR-2011738. The Flatiron Institute is a division of the Simons Foundation.

[1] X.-L. Qi and S.-C. Zhang, Topological insulators and superconductors, Reviews of Modern Physics **83**, 1057 (2011).
[2] C. Nayak, S. H. Simon, A. Stern, M. Freedman, and S. D. Sarma, Non-abelian anyons and topological quantum computation, Reviews of Modern Physics **80**, 1083 (2008).
[3] N. Read and D. Green, Paired states of fermions in two dimensions with breaking of parity and time-reversal symmetries and the fractional quantum hall effect, Physical Review B **61**, 10267 (2000).
[4] M. Sato and Y. Ando, Topological superconductors: a review, Reports on Progress in Physics **80**, 076501 (2017).
[5] M. Leijnse and K. Flensberg, Introduction to topological superconductivity and majorana fermions, Semiconductor Science and Technology **27**, 124003 (2012).
[6] V. Crépel, B. Estienne, and N. Regnault, Variational ansatz for an abelian to non-abelian topological phase transition in ν= 1/2+ 1/2 bilayers, Physical Review Letters **123**, 126804 (2019).
[7] K. Flensberg, F. von Oppen, and A. Stern, Engineered platforms for topological superconductivity and majorana zero modes, Nature Reviews Materials **6**, 944 (2021).
[8] J. Alicea, New directions in the pursuit of majorana fermions in solid state systems, Reports on progress in physics **75**, 076501 (2012).
[9] P. Sharma, N. Karn, V. S. Awana, et al., A comprehensive review on topological superconducting materials and interfaces, Superconductor Science and Technology (2022).
[10] Y. S. Hor, A. J. Williams, J. G. Checkelsky, P. Roushan, J. Seo, Q. Xu, H. W. Zandbergen, A. Yazdani, N. P. Ong, and R. J. Cava, Superconductivity in cu x bi 2 se 3 and its implications for pairing in the undoped topological insulator, Physical review letters **104**, 057001 (2010).
[11] L. Fu and E. Berg, Odd-parity topological superconductors: theory and application to cu x bi 2 se 3, Physical review letters **105**, 097001 (2010).
[12] G. Xu, B. Lian, P. Tang, X.-L. Qi, and S.-C. Zhang, Topological superconductivity on the surface of fe-based superconductors, Physical review letters **117**, 047001 (2016).

[13] P. Zhang, K. Yaji, T. Hashimoto, Y. Ota, T. Kondo, K. Okazaki, Z. Wang, J. Wen, G. Gu, H. Ding, et al., Observation of topological superconductivity on the surface of an iron-based superconductor, Science **360**, 182 (2018).

[14] D. Wang, L. Kong, P. Fan, H. Chen, S. Zhu, W. Liu, L. Cao, Y. Sun, S. Du, J. Schneeloch, et al., Evidence for majorana bound states in an iron-based superconductor, Science **362**, 333 (2018).

[15] P. Zhang, Z. Wang, X. Wu, K. Yaji, Y. Ishida, Y. Kohama, G. Dai, Y. Sun, C. Bareille, K. Kuroda, et al., Multiple topological states in iron-based superconductors, Nature Physics **15**, 41 (2019).

[16] Y. Cao, V. Fatemi, S. Fang, K. Watanabe, T. Taniguchi, E. Kaxiras, and P. Jarillo-Herrero, Unconventional superconductivity in magic-angle graphene superlattices, Nature **556**, 43 (2018).

[17] J. M. Park, Y. Cao, L.-Q. Xia, S. Sun, K. Watanabe, T. Taniguchi, and P. Jarillo-Herrero, Robust superconductivity in magic-angle multilayer graphene family, Nature Materials **21**, 877 (2022).

[18] L. Balents, C. R. Dean, D. K. Efetov, and A. F. Young, Superconductivity and strong correlations in moiré flat bands, Nature Physics **16**, 725 (2020).

[19] B. Estienne, N. Regnault, and V. Crépel, Ideal chern bands are landau levels in curved space, arXiv preprint arXiv:2304.01251 (2023).

[20] E. Y. Andrei, D. K. Efetov, P. Jarillo-Herrero, A. H. MacDonald, K. F. Mak, T. Senthil, E. Tutuc, A. Yazdani, and A. F. Young, The marvels of moiré materials, Nature Reviews Materials **6**, 201 (2021).

[21] V. Crépel, N. Regnault, and R. Queiroz, The chiral limits of moir\'e semiconductors: origin of flat bands and topology in twisted transition metal dichalcogenides homobilayers, arXiv preprint arXiv:2305.10477 (2023).

[22] K. F. Mak and J. Shan, Semiconductor moiré materials, Nature Nanotechnology **17**, 686 (2022).

[23] F. Wu, T. Lovorn, E. Tutuc, I. Martin, and A. MacDonald, Topological insulators in twisted transition metal dichalcogenide homobilayers, Physical review letters **122**, 086402 (2019).

[24] V. Crépel and L. Fu, Anomalous hall metal and fractional chern insulator in twisted transition metal dichalcogenides, arXiv preprint arXiv:2207.08895 (2022).

[25] T. Devakul, V. Crépel, Y. Zhang, and L. Fu, Magic in twisted transition metal dichalcogenide bilayers, Nature communications **12**, 1 (2021).

[26] W. Zhao, B. Shen, Z. Tao, Z. Han, K. Kang, K. Watanabe, T. Taniguchi, K. F. Mak, and J. Shan, Gate-tunable heavy fermions in a moir\'e kondo lattice, arXiv preprint arXiv:2211.00263 (2022).

[27] A. Kumar, N. C. Hu, A. H. MacDonald, and A. C. Potter, Gate-tunable heavy fermion quantum criticality in a moiré kondo lattice, Physical Review B **106**, L041116 (2022).

[28] A. Dalal and J. Ruhman, Orbitally selective mott phase in electron-doped twisted transition metal-dichalcogenides: A possible realization of the kondo lattice model, Physical Review Research **3**, 043173 (2021).

[29] D. Guerci, J. Wang, J. Zang, J. Cano, J. H. Pixley, and A. Millis, Chiral kondo lattice in doped $mote_2/wse_2$ bilayers, Science Advances **9**, eade7701 (2023), https://www.science.org/doi/pdf/10.1126/sciadv.ade7701.

[30] I. Schwartz, Y. Shimazaki, C. Kuhlenkamp, K. Watanabe, T. Taniguchi, M. Kroner, and A. Imamoğlu, Electrically tunable feshbach resonances in twisted bilayer semiconductors, Science **374**, 336 (2021).

[31] C. Chin, R. Grimm, P. Julienne, and E. Tiesinga, Feshbach resonances in ultracold gases, Reviews of Modern Physics **82**, 1225 (2010).

[32] C. Kuhlenkamp, M. Knap, M. Wagner, R. Schmidt, and A. Imamoğlu, Tunable feshbach resonances and their spectral signatures in bilayer semiconductors, Physical Review Letters **129**, 037401 (2022).

[33] Z. Sun, J. Beaumariage, Q. Wan, H. Alnatah, N. Hougland, J. Chisholm, Q. Cao, K. Watanabe, T. Taniguchi, B. M. Hunt, et al., Charged bosons made of fermions in bilayer structures with strong metallic screening, Nano Letters **21**, 7669 (2021).

[34] C. Regal, C. Ticknor, J. L. Bohn, and D. S. Jin, Tuning p-wave interactions in an ultracold fermi gas of atoms, Physical review letters **90**, 053201 (2003).

[35] J. Zhang, E. Van Kempen, T. Bourdel, L. Khaykovich, J. Cubizolles, F. Chevy, M. Teichmann, L. Tarruell, S. Kokkelmans, and C. Salomon, P-wave feshbach resonances of ultracold li 6, Physical Review A **70**, 030702 (2004).

[36] K. Günter, T. Stöferle, H. Moritz, M. Köhl, and T. Esslinger, p-wave interactions in low-dimensional fermionic gases, Physical review letters **95**, 230401 (2005).

[37] J. Gaebler, J. Stewart, J. Bohn, and D. Jin, p-wave feshbach molecules, Physical review letters **98**, 200403 (2007).

[38] F. Ç. Top, Y. Margalit, and W. Ketterle, Spin-polarized fermions with p-wave interactions, Physical Review A **104**, 043311 (2021).

[39] J. J. Park, Y.-K. Lu, A. O. Jamison, T. V. Tscherbul, and W. Ketterle, A feshbach resonance in collisions between triplet ground-state molecules, Nature **614**, 54 (2023).

[40] M. Randeria, J.-M. Duan, and L.-Y. Shieh, Superconductivity in a two-dimensional fermi gas: Evolution from cooper pairing to bose condensation, Physical Review B **41**, 327 (1990).

[41] Y.-C. Zhang and S. Zhang, Strongly interacting p-wave fermi gas in two dimensions: Universal relations and breathing mode, Physical Review A **95**, 023603 (2017).

[42] T. Senthil and M. P. A. Fisher, Z_2 gauge theory of electron fractionalization in strongly correlated systems, Phys. Rev. B **62**, 7850 (2000).

[43] Z. Nussinov and G. Ortiz, Autocorrelations and thermal fragility of anyonic loops in topologically quantum ordered systems, Physical Review B **77**, 064302 (2008).

[44] X.-L. Qi, T. L. Hughes, S. Raghu, and S.-C. Zhang, Time-reversal-invariant topological superconductors and superfluids in two and three dimensions, Physical review letters **102**, 187001 (2009).

[45] D. Guerci, V. Crépel, J. Cano, J. H. Pixley, and A. Millis, in preparation (2023).

[46] A. Altland and M. R. Zirnbauer, Nonstandard symmetry classes in mesoscopic normal-superconducting hybrid structures, Physical Review B **55**, 1142 (1997).

[47] F. Pizzocchero, L. Gammelgaard, B. S. Jessen, J. M. Caridad, L. Wang, J. Hone, P. Bøggild, and T. J. Booth, The hot pick-up technique for batch assembly of van der waals heterostructures, Nature communications **7**, 1 (2016).

[48] C. Zhang, C. Gong, Y. Nie, K.-A. Min, C. Liang, Y. J. Oh, H. Zhang, W. Wang, S. Hong, L. Colombo, et al., Systematic study of electronic structure and band alignment of monolayer transition metal dichalcogenides in van der waals heterostructures, 2D Materials **4**, 015026 (2016).

[49] S. Carr, D. Massatt, S. B. Torrisi, P. Cazeaux, M. Luskin, and E. Kaxiras, Relaxation and domain formation in incommensurate two-dimensional heterostructures, Physical Review B **98**, 224102 (2018).

[50] D. Massatt, S. Carr, and M. Luskin, Electronic observables for relaxed bilayer 2d heterostructures in momentum space, arXiv preprint arXiv:2109.15296 (2021).

[51] Y. Zhang, T. Devakul, and L. Fu, Spin-textured chern bands in ab-stacked transition metal dichalcogenide bilayers, Proceedings of the National Academy of Sciences **118**, e2112673118 (2021).

[52] L. Rademaker, Spin-orbit coupling in transition metal dichalcogenide heterobilayer flat bands, Physical Review B **105**, 195428 (2022).

[53] H. Pan, M. Xie, F. Wu, and S. D. Sarma, Topological phases in ab-stacked mote 2/wse 2: Z 2 topological insulators, chern insulators, and topological charge density waves, Physical Review Letters **129**, 056804 (2022).

[54] A. Kormányos, G. Burkard, M. Gmitra, J. Fabian, V. Zólyomi, N. D. Drummond, and V. Fal'ko, k· p theory for two-dimensional transition metal dichalcogenide semiconductors, 2D Materials **2**, 022001 (2015).

[55] T. Li, S. Jiang, B. Shen, Y. Zhang, L. Li, Z. Tao, T. Devakul, K. Watanabe, T. Taniguchi, L. Fu, et al., Quantum anomalous hall effect from intertwined moiré bands, Nature **600**, 641 (2021).

[56] W. Zhao, K. Kang, L. Li, C. Tschirhart, E. Redekop, K. Watanabe, T. Taniguchi, A. Young, J. Shan, and K. F. Mak, Realization of the haldane chern insulator in a moir\'e lattice, arXiv preprint arXiv:2207.02312 (2022).

[57] See supplementary materials at url.

[58] K. Slagle and L. Fu, Charge transfer excitations, pair density waves, and superconductivity in moiré materials, Phys. Rev. B **102**, 235423 (2020).

[59] V. Crépel and L. Fu, New mechanism and exact theory of superconductivity from strong repulsive interaction, Science Advances **7**, eabh2233 (2021).

[60] V. Crépel and L. Fu, Spin-triplet superconductivity from excitonic effect in doped insulators, Proceedings of the National Academy of Sciences **119**, e2117735119 (2022).

[61] V. Crépel, T. Cea, L. Fu, and F. Guinea, Unconventional superconductivity due to interband polarization, Physical Review B **105**, 094506 (2022).

[62] Y. He, K. Yang, J. B. Hauck, E. J. Bergholtz, and D. M. Kennes, Superconductivity of repulsive spinless fermions with sublattice potentials, Physical Review Research **5**, L012009 (2023).

[63] S. Maiti and A. V. Chubukov, Superconductivity from repulsive interaction, in AIP Conference Proceedings, Vol. 1550 (American Institute of Physics, 2013) pp. 3–73.

[64] We fixed the unit cell area to one.

[65] A. P. Schnyder, S. Ryu, A. Furusaki, and A. W. Ludwig, Classification of topological insulators and superconductors in three spatial dimensions, Physical Review B **78**, 195125 (2008).

[66] C. Kallin and J. Berlinsky, Chiral superconductors, Reports on Progress in Physics **79**, 054502 (2016).

[67] B. Jäck, Y. Xie, and A. Yazdani, Detecting and distinguishing majorana zero modes with the scanning tunnelling microscope, Nature Reviews Physics **3**, 541 (2021).

[68] A. Leggett, Number-phase fluctuations in two-band superconductors, Progress of Theoretical Physics **36**, 901 (1966).

[69] V. Gurarie, L. Radzihovsky, and A. Andreev, Quantum phase transitions across a p-wave feshbach resonance, Physical review letters **94**, 230403 (2005).

[70] M. Randeria and E. Taylor, Crossover from bardeen-cooper-schrieffer to bose-einstein condensation and the unitary fermi gas, Annu. Rev. Condens. Matter Phys. **5**, 209 (2014).

[71] V. Gurarie and L. Radzihovsky, Resonantly paired fermionic superfluids, Annals of Physics **322**, 2 (2007).

[72] M. Z. Hasan and C. L. Kane, Colloquium: topological insulators, Reviews of modern physics **82**, 3045 (2010).

[73] J. Levinsen and M. M. Parish, Strongly interacting two-dimensional fermi gases, Annual review of cold atoms and molecules , 1 (2015).

Supplementary material for: " Topological superconductivity in doped magnetic moiré semiconductors"

Valentin Crépel[1] , Daniele Guerci[1], Jennifer Cano[2,1], J. H. Pixley[3,1], Andrew Millis[4,1]
[1] *Center for Computational Quantum Physics, Flatiron Institute, New York, New York 10010, USA*
[2] *Department of Physics and Astronomy, Stony Brook University, Stony Brook, New York 11794, USA*
[3] *Department of Physics and Astronomy, Center for Materials Theory, Rutgers University, Piscataway, New Jersey 08854, USA*
[4] *Department of Physics, Columbia University, New York, NY 10027, USA*

These supplementary materials contain the details of analytic calculations as well as additional numerical details supporting the results presented in the main text. It is structured as follows. In Sec. A we discuss the Schrieffer-Wolff transformation providing the effective lattice model describing the doped charges' dynamics, and expand it in the low density limit, which gives rise to the low-energy theory presented in the main text. In Sec. B and C we discuss the $2e$ bound states forming the dilute BEC and the expression for T^* in the BCS regime, respectively. Finally, in Sec. D we comment on a quartic symmetry allowed term coupling the density $|\phi_+|$ and $|\phi_-|$ of the two spin-valley locked condensates.

Appendix A: Schrieffer-Wolff transformation

In this section we detail the effective Hamiltonian of itinerant carriers hybridizing with the ferromagnetically ordered moments. We perform an expansion in the interlayer parameter t_{ud}, which we recall is small compared to the charge transfer gap Δ.

1. Effective lattice model

Accounting for all possible virtual processes we find that the lattice Hamiltonian for the doped charges reads

$$\begin{aligned} H_{\text{eff}} = &- t_{uu} \sum_{\langle i,j\rangle_{ab}} c_i^\dagger e^{-i\sigma^z \nu_{ij}^{uu}\varphi} c_j + U_u \sum_i n_{i\uparrow} n_{i\downarrow} \\ &+ \sum_{ijk\in\triangle}^{i\neq j\neq k} \left\{ c_i^\dagger \left[\boldsymbol{S}_A \cdot \boldsymbol{\sigma} + \frac{1}{2} \right] (t_K + \lambda n_k) c_j + P_{ijk} \right\} + \left[U_2 + U_3 \frac{n_\triangle - 2}{3} \right] \frac{n_\triangle (n_\triangle - 1)}{2} , \end{aligned} \tag{A1}$$

where $n_\triangle = n_i + n_j + n_k$ is the total density on the lower triangles $\triangle$ forming the u lattice, P_{ijk} denotes summation over all permutation of the indices ijk, and $[\boldsymbol{S}_A \cdot \boldsymbol{\sigma} + 1/2]$ describes the exchange of spin between the u carriers and the nearest d spin. Finally, we replace the spin operators $\boldsymbol{S}_A$ by their classical values $\boldsymbol{S}_A \to \langle \boldsymbol{S}_A \rangle$ assuming long-range magnetic order in the d layer and neglecting low-energy spin wave excitations. Setting $t = t_{ud}$, the coefficients appearing in H_{eff} A1 are

$$t_K = \frac{t^2}{\Delta + V}, \quad \lambda = \frac{t^2}{\Delta} - \frac{t^2}{\Delta + V}, \quad U_2 = -\frac{t^2}{\Delta} + \frac{4t^2}{\Delta + V} - \frac{3t^2}{\Delta + 2V}, \quad U_3 = \frac{3t^2}{\Delta} - \frac{6t^2}{\Delta + V} + \frac{3t^2}{\Delta + 2V}. \tag{A2}$$

2. Low-energy projection

At low density of doped carriers in the u layer we expand Eq. A1 close to the bottom of the itinerant band by retaining only the spin-valley locked fermionic modes at a distance $|q| \ll 1$ from the $\pm\kappa$ points, gathered in the spinor $\tilde{\Psi}_q = (\psi_{q,\Uparrow}, \psi_{q,\Downarrow})^T$ with $\Uparrow$ / $\Downarrow$= $(\kappa/\kappa', \uparrow$ / $\downarrow)$. The kinetic part of the Hamiltonian is simply $q^2/2m$ with $m^{-1} = 9(t_K + 4t_{uu})/4$. Moreover, the interaction coefficients in Eq. 3 of the manuscript read $g_s = U + 6U_2 - 3\lambda$, $g_t = 9(\lambda - 4U_2)/8$, $g_t' = 27\lambda/8$, where λ and U_2 are given in Eq. A2.

Appendix B: Two doped charges

The binding energy B_2 shown in Fig. 4b are obtained by solving the effective tight-binding model Eq. A1 for zero, one and two particles. In the last case, we decouple the center of mass and the relative motion to access larger system sizes.

The solid black line in Fig. 4b showing the separation between the regions with and without bound states is obtained looking for the poles of the T matrix [73]:

$$-\frac{1}{g_t + g_t'} = \Pi_t(-|\epsilon|), \tag{B1}$$

where the polarization bubble takes the form:

$$\Pi_t(-|\epsilon|) = \int^{\Lambda} \frac{d^2k}{(2\pi)^2} \frac{k^2}{|\epsilon| + k^2/2m}, \tag{B2}$$

where $\epsilon = -|\epsilon| < 0$ is negative and Λ is the UV cutoff. The value of Λ is obtained by fitting the numerical results from the lattice model.

Appendix C: Pair binding energy

Our weak coupling estimate for T^* is obtained by solving

$$1 = -[g_t + g_t']\chi_t(T^*), \tag{C1}$$

where the triplet susceptibility reads

$$\chi_t(T) = \int^{\Lambda} \frac{d^2k}{2\pi^2} \frac{k^2}{k^2/2m - \mu} \tanh \frac{k^2/2m - \mu}{2T}. \tag{C2}$$

In the latter expression the chemical potential is fixed by:

$$x = \int^{\Lambda} \frac{d^2k}{2\pi^2} f\left(\frac{k^2}{2m} - \mu\right). \tag{C3}$$

with f the Fermi-Dirac distribution. Finally, we also give the expression for the $T = 0$ superconducting gap equation:

$$1 = -(g_t + g_t') \int^{\Lambda} \frac{d^2k}{4\pi^2} \frac{k^2}{\sqrt{(k^2/2m - \mu)^2 + |\phi|^2 k^2}}, \tag{C4}$$

with $|\phi| = |\phi_+^+| = |\phi_-^-|$.

Appendix D: Symmetry allowed quartic term in GL free energy

Including longer range interactions can mix the two order parameters ϕ_+ and ϕ_- at the quartic level through a correction of the Ginzburg-Landau free energy $\delta\mathcal{F} = \beta|\phi_+\phi_-|^2$. Alll other quartic terms mixing the two superconducting orders involve large momentum transfer $\pm\kappa$ and thus average to zero. Including the dominant intra- and inter- layer interactions yields $\beta = 0$ (see main text), and we expect that the sub-dominant interactions discarded in our model Eqs. 1&2 will keep the β coefficient small compared to one. In particular, so long as $\beta < 2$, we will continue to have $|\phi_+| = |\phi_-|$ and all the results derived in the main text remain valid.